

Robust Attitude Control of a Flexible Launch Vehicle Subjected to Wind Disturbances

Andréa F. C. de S. Yamada* Karl H. Kienitz**
Fausto de O. Ramos***

* *Instituto de Fomento e Coordenação Industrial, São José dos Campos, São Paulo, Brasil*
(e-mail: andreaferazafcsy@fab.mil.br)

** *Instituto Tecnológico de Aeronáutica, São José dos Campos, São Paulo, Brasil* (e-mail: kienitz@ita.br)

*** *Instituto de Aeronáutica e Espaço, São José dos Campos, São Paulo, Brasil* (e-mail: faustofor@fab.mil.br)

Abstract: The attitude control and robust performance problems are herein investigated for a coupled 3DOF launch vehicle system that includes flexible modes and nonlinear actuators. Although atmospheric conditions like wind and the transonic flight are extreme, the robust control design is efficient even for an asymmetric time-varying plant updated at each iteration during 50 seconds of simulation. A two-degree-of-freedom topology known as Kreisselmeier's structure, in which a TFL/LTR compensator is inserted, adding robustness to the control loop, satisfies the time domain requirements. The present work focuses on the time response and the low-frequency specifications of the Brazilian VLS rocket.

Keywords: attitude control; robustness; launch vehicle; flexible modes; time-varying plant.

1. INTRODUCTION

The attitude control of a satellite launch vehicle during the ascending trajectory is a defiant problem once the body's natural flexible modes are considered in addition to the unstable and time-varying dynamics. Moreover, the atmospheric conditions modify the plant parameters during the flight and the wind is a disturbance to the system. Another difficulty in the design is the limited deflection of the actuators. Many robust control methods have been applied in the control study for launch vehicles whose payloads vary from 10 (kg) (a nanosatellite) to around 2 (tons), as shown by Mooij (2020), Navarro-Tapia et al. (2016), Lu et al. (2015), Dubanchet et al. (2012), Ganet-Schoeller and Ducamp (2010).

The Brazilian VLS launch is proposed to insert a 380 (kg) payload in Low Earth Orbit (LEO). The vehicle has a solid propeller that accelerates continuously in its longitudinal axis since the thrust force cannot be controlled. During the first stage of flight, the rocket attitude is modified by its nozzles deflection, which is known as Thrust Vector Control (TVC), as detailed and illustrated in Leite Filho (2002), Ramos (2011) and Palmério (2017). The problem consists of stabilizing and controlling the system, maintaining the vehicle the nearest as possible to its ideal trajectory, which means satisfying the quite critical requirements of attitude reference tracking in the three axes of the body. Furthermore, the control strategy applied can attenuate the body bending modes to keep the rocket's stability, as also to get along with the wind disturbance and the time-varying plant parameters. The results herein presented consider a coupled 3DOF (Three Degrees of Freedom) asymmetric and flexible launch model with 3 ($^{\circ}$) of limit in actuation. The compensator proposed also attenuates the body's natural frequencies itself, discarding the necessity of a bending filter.

The robust stability ensures that the compensator can maintain the stability for a broader range of time because not only the nominal system is stable, but also a class of perturbed systems (Skogestad and Postlethwaite, 1996). So, the mismatches between the nominal model and the real plant may be analyzed as a group of perturbed models (Cruz, 1996). That concept may be expanded for time-varying systems once the plant operating conditions are different from the nominal operating point.

The novel contribution in this work is the combination of Kreisselmeier's topology with a TFL/LTR (Target Feedback Loop / Loop Transfer Recovery) compensator for a launch vehicle. The TFL/LTR embraces the conventional LQG/LTR (Linear Quadratic Gaussian) and its variations, as detailed in Prakash (1990). Such procedures apply the Kalman filter and regulator theories as convenient ways to calculate the gains of the compensator. Also, two loop structures are evaluated: the conventional and the called "small gain", which diminishes the amplitude of the needed control signal. Two operating points are defined to calculate the compensator gains: at 1 (s) of flight and the instant of maximum dynamic pressure. Besides that, a simplified TFL/LTR algorithm is used for actualizing the gains at the instant of 20 (s) of flight. Kreisselmeier's topology with two degrees of freedom allows to impose input-output behavior in the time domain and, additionally, disturbance rejection in the frequency domain, as demonstrated by Kienitz and Kadirkamanathan (2017).

The step time response demands are fulfilled with no overshoot, and the trajectory following requirements are satisfied even during the transonic regime. Finally, the robustness in low frequencies is verified for wind step, that is attenuated simultaneously in pitch and yaw.

In the next section, the flexible body coupled nonlinear model is presented, and, in sequence, the control theory and the design are discussed, followed by the evaluation and conclusion of the results.

2. THREE DEGREES OF FREEDOM LAUNCH VEHICLE MODEL

The Brazilian Satellite Launch Vehicle (VLS) model follows the conventions shown in Fig. 1, where (X_b, Y_b, Z_b) is the body-referenced trihedron, V is the body velocity vector and F_{Ez} is the thrust force in axis Z .

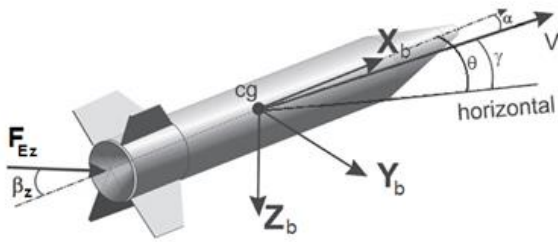


Fig. 1. Body system convention (Palmério, 2017).

2.1 Rigid body coupled linear model

The rigid body linear dynamic is unstable in the selected operating points. The eighth-order linear model (1) is obtained considering the linear axial velocity as a constant ($u = \bar{U}$) for each operating point, whose states are $x = [w \ q \ \theta \ v \ r \ \psi \ p \ \phi]^T$, as described in the work of Ramos (2011). The system outputs are the Euler angles for pitch, yaw, and roll, respectively, $y = Cx = [\theta \ \psi \ \phi]^T$. The matrices B_u and B_d are defined individually to separate the effects of control effort $u = [\beta_z \ \beta_y \ \beta_r]^T$ from those of wind disturbance $d = [v_w \ w_w]^T$.

$$\dot{x} = Ax + [B_u \ B_d] \begin{bmatrix} u \\ d \end{bmatrix} = Ax + B \begin{bmatrix} u \\ d \end{bmatrix} \quad (1)$$

2.2 Flexible body coupled nonlinear model

The flexible system is composed of the ninth-order rigid body nonlinear dynamic displayed from (2) to (10), which incorporates Coriolis terms. Appended to the nonlinear equations, are the nonlinear actuators in the three planes of motion plus the bending modes in the yaw and pitch planes:

$$\dot{u} = -\frac{C_{drag} P_d S_{ref}}{m} + \frac{F_{Ex}}{m} + v r - w q - g \cos(\theta) \cos(\psi) \quad (2)$$

$$\dot{v} = -Y_\beta \beta + Y_{\beta_y} \beta_y - \left(\frac{2 \dot{m} x_e}{m} + u \right) r + w p + v_1 \quad (3)$$

$$\dot{w} = -Z_\alpha \alpha + Z_{\beta_z} \beta_z + \left(\frac{2 \dot{m} x_e}{m} + u \right) q - v p + w_1 \quad (4)$$

$$\dot{p} = -L_p p + L_{\beta_x} \beta_x + \frac{I_{yy} I_{zz}}{I_{xx}} q r \quad (5)$$

$$\dot{q} = M_\alpha \alpha - M_{\beta_z} \beta_z - M_q q - \frac{I_{xx} I_{zz}}{I_{yy}} p r \quad (6)$$

$$\dot{r} = -N_\beta \beta + N_{\beta_y} \beta_y - N_r r + \frac{I_{xx} I_{yy}}{I_{zz}} p q \quad (7)$$

$$\dot{\theta} = \frac{\cos(\phi)}{\cos(\psi)} q - \frac{\sin(\phi)}{\cos(\psi)} r \quad (8)$$

$$\dot{\psi} = \sin(\phi) q + \cos(\phi) r \quad (9)$$

$$\dot{\phi} = p - \tan(\psi) \cos(\phi) q + \tan(\psi) \sin(\phi) r \quad (10)$$

where

$$v_1 = -g \sin(\theta) \sin(\phi) + g \cos(\theta) \sin(\psi) \cos(\phi)$$

$$w_1 = -g \sin(\theta) \cos(\phi) - g \cos(\theta) \sin(\psi) \sin(\phi)$$

The flexible modes are described by a second-order dynamic that overlaps the nonlinear rigid body parameters above for pitch and yaw axes, as illustrated for the pitch axis in Fig. 2 and described in (11) and (12), where $q_{rb}=q$, $\theta_{rb}=\theta$ and $i=1,2$ indicates the mode (first or second). The damping factor ζ is a constant, while the gain K_B and the frequency ω_B vary with the operating point, originating the frequencies that constitute each mode.

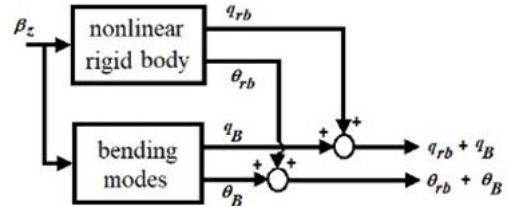


Fig. 2. Bending modes for pitch plane (Moreira, 1995).

$$\dot{x}_{Bi} = A_{Bi} x_{Bi} + B_{Bi} \beta_z \rightarrow$$

$$\begin{bmatrix} \dot{\theta}_{Bi} \\ \dot{q}_{Bi} \end{bmatrix} = \begin{bmatrix} 0 & 1 \\ -\omega_{Bi}^2 & -2\zeta\omega_{Bi} \end{bmatrix} \begin{bmatrix} \theta_{Bi} \\ q_{Bi} \end{bmatrix} + \begin{bmatrix} 0 \\ K_{Bi} \end{bmatrix} \beta_z \quad (11)$$

$$y_{Bi} = Cx_{Bi} \rightarrow \begin{bmatrix} \theta_{Bi} \\ q_{Bi} \end{bmatrix} = \begin{bmatrix} 1 & 0 \\ 0 & 1 \end{bmatrix} \begin{bmatrix} \theta_{Bi} \\ q_{Bi} \end{bmatrix} \quad (12)$$

3. ROBUST CONTROLLER

Robust performance specifications can be expressed as barriers in the frequency domain since disturbances that vary fast in time, like sensors noise and bending modes, are positioned in the high-frequency range; while, by contrast, wind, reference tracking, and perturbations in plant parameters, which change slowly in time, take place in low frequencies (Cruz, 1996). Accordingly, the gains of compensator $K(s)$ are modified graphically in the frequency domain using the loop shaping approach that consists in modeling the singular values of the multivariable loop transfer function $G(j\omega)K(j\omega)$. To accomplish the design trade-offs, the barrier in low frequencies cannot be disobeyed by the lowest singular value of $G(s)K(s)$, as well as the barrier in high frequencies cannot be broken by its highest singular value (Fig. 3). The one degree of freedom loop subjected to the references r and perturbations in low and high frequencies bandwidth, respectively, d and n , is illustrated in Fig. 4. Next, the frequency specifications are briefly presented since they are developed in detail in Cruz (1996) and Yamada (2019).

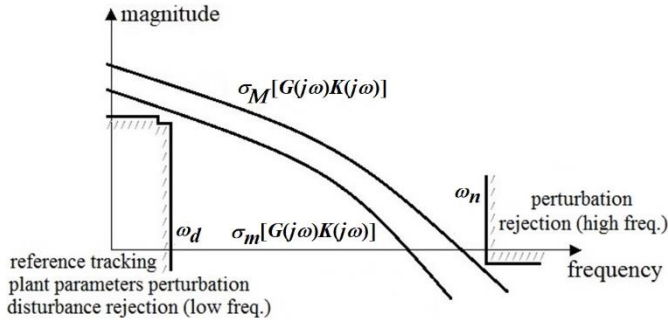


Fig. 3. Robust performance barriers of the nominal system.

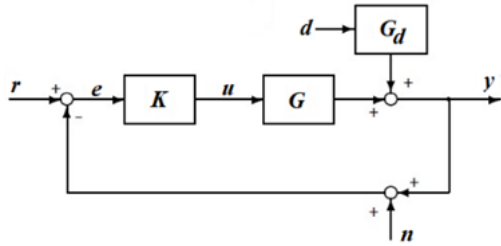


Fig. 4. One degree of freedom robust control structure (Skogestad and Postlethwaite, 1996).

If region Ω_d contains the major part of disturbances in low frequency, the function $\alpha_d(\omega)$ can be defined as the disturbance rejection specification. In that way, the minimal singular value σ_m of $[I + G(j\omega)K(j\omega)]$ must respect the barrier $1/\alpha_d(\omega)$, which is commonly used in the simplified form written in (13). Therefore, the stated barrier cannot be violated by the minimal singular value of the nominal loop transfer matrix $G(j\omega)K(j\omega)$.

$$\sigma_m[G(j\omega)K(j\omega)] \geq \frac{1}{\alpha_d(\omega)} \gg 1, \quad (13)$$

with $\omega \in \Omega_d$, $\Omega_d = \{\omega \in R \mid \omega \leq \omega_d\}$

In an analogous form, the function $\alpha_n(\omega)$ can be defined as the perturbation rejection specification for high frequencies. So, the stated barrier cannot be violated by the maximal singular value σ_M of the nominal loop transfer matrix $G(j\omega)K(j\omega)$.

$$\sigma_M[G(j\omega)K(j\omega)] \leq \alpha_n(\omega) \ll 1, \quad (14)$$

since $\omega \in \Omega_n$, $\Omega_n = \{\omega \in R \mid \omega \geq \omega_n\}$

3.1 The TFL/LTR Procedure

The TFL/LTR method consists in selecting the gains of a multiple-input multiple-output linear time-invariant compensator K that satisfies the robust barriers specification.

The nominal plant G_p described in (15) is a LTI system with n states ($x_p \in R^n$), m inputs ($u_p \in R^m$), and m outputs ($y_p \in R^m$).

$$\begin{cases} \dot{x}_p = A_p x_p + B_p u_p \\ y = C_p x_p \end{cases}$$

$$G_p(s) = C_p(sI - A_p)^{-1} B_p \quad (15)$$

In the present work, one integrator is added before each input

of the plant to improve the shaping of the target singular values, leading to the augmented dynamic G (16) with $(n+m)$ states, m inputs, and m outputs (Prakash, 1990). The integral action is indeed part of controller K , despite the gains calculated using G (Fig. 5).

$$\begin{cases} \dot{x} = Ax + Bu \\ y = Cx \end{cases}$$

$$A = \begin{bmatrix} A_p & B_p \\ 0 & 0 \end{bmatrix} \quad B = \begin{bmatrix} 0 \\ I \end{bmatrix} \quad C = [C_p \quad 0]$$

$$G(s) = (I/s)G_p(s) = C(sI - A)^{-1}B \quad (16)$$

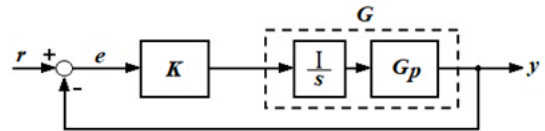


Fig. 5. The integral action is treated as part of the plant during the design of compensator K .

The conventional TFL/LTR structure (Fig. 6) is composed of two loops, whose matrices K_f and K_r are the design variables, and the augmented matrices A , B , and C are fixed in the plant $z \in R^{n+m}$ and the transfer function is given in (17).

$$\begin{cases} \dot{z} = Az + Bu + K_f(-e - Cz) = (A - K_f C - BK_r)z - K_f e \\ u = -K_r z = Ke \end{cases}$$

$$K(s) = K_r(sI - A + K_f C + BK_r)^{-1} K_f \quad (17)$$

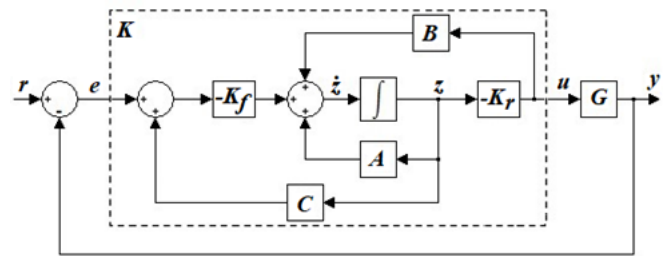


Fig. 6. Conventional structure of TFL/LTR compensator.

In the LTR step of the method, the recovery of singular values is accelerated, excluding the matrix C loop of the conventional structure, as proposed by Prakash (1990). This results in the small gain alternative (Fig. 7) and, in terms of equations, it means removing $K_f C$ from (17):

$$\begin{cases} \dot{z} = Az + Bu - K_f e = (A - BK_r)z - K_f e \\ u = -K_r z = Ke \end{cases}$$

$$K(s) = K_r(sI - A + BK_r)^{-1} K_f \quad (18)$$

Independently on the structure, matrices $(A - K_f C)$ and $(A - BK_r)$ are necessarily stables since K_f is calculated as the gains of a Kalman filter $\dot{\hat{z}} = (A - K_f C)\hat{z} + Bu - K_f y$ and K_r , as an LQR regulator $u = -K_r z$ (Prakash, 1990). Thus, the small gain choice

is always stable once its poles are the eigenvalues of $(A - BK_r)$. Nevertheless, matrix $(A - K_f C - BK_r)$ may be unstable. Next, the steps of TFL/LTR procedure are briefly explained.

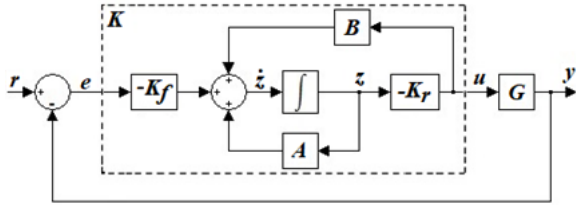


Fig. 7. Small gain structure of TFL/LTR compensator.

3.1.1 Target Feedback Loop (TFL)

In the perturbations-reflected-to-output (PRO) version of the TFL/LTR procedure, the performance is evaluated at the output point of the plant. Hence, the TFL loop (Fig. 8) contains the parameter K_f , whose values determine the shape of the singular values of the target feedback loop transfer function G_{KF} given in (19).

$$G_{KF}(s) = C(sI - A)^{-1}K_f \quad (19)$$

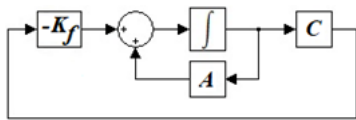


Fig. 8. TFL loop in the PRO version of TFL/LTR.

The gains K_f are calculated through (21) and Riccati equation (20), whose solution is the symmetric positive semi-definite matrix P . The parameters of (20) and (21) are the plant dynamic G , the symmetric positive semi-definite matrix $Q = LL^T$, and the diagonal symmetric positive definite matrix $R = \mu I_m$, with $\mu > 0$ and m equal to the outputs of the system.

$$AP + PA^T + Q - PC^T R^{-1} CP = 0 \quad (20)$$

$$K_f = R^{-1} C^T P \quad (21)$$

Robust specifications normally demand $\sigma_m[G_{KF}(j\omega)] \gg 1$ in low frequencies and matched singular values ($\sigma_m = \sigma_M$) in all frequency ranges. Therefore, G_{KF} depends on the adjustment of parameters μ and L , as expressed in Kalman Identity (22). Parameter μ moves vertically the singular values of G_{KF} (the lower μ , the higher the magnitude of the singular values). The poles of $C(sI - A)^{-1}L$ are defined by matrix A and are placed according to the operating point of the plant. So, the shape of G_{KF} is modified through transmission zeros that lay on matrix L .

$$\sigma_i[G_{KF}(j\omega)] \cong \frac{1}{\sqrt{\mu}} \sigma_i[C(sI - A)^{-1}L] \quad (22)$$

Partitioning $L^{[(n+m) \times m]}$ as in (23) (Athans 1986), matched singular values can be obtained in low and high frequencies, because the shape of the singular values in low frequencies is influenced by $L_L^{(n \times m)}$ and, in high frequencies, by $L_H^{(m \times m)}$.

$$L = [L_L \quad L_H]^T,$$

$$\text{with } L_L = -(C_p A_p^{-1} B_p)^{-1}, \quad L_H = C_p^T (C_p C_p^T)^{-1} \quad (23)$$

3.1.2 Loop Transfer Recovery (LTR)

The loop recovery transfer function GK is evaluated in the output of the controller and approximates G_{KF} through the adjustment of gains K_r . According to Doyle and Stein (1981), GK tends point-to-point to the target G_{KF} , as the parameter p decreases positively.

The solution of Riccati equation (24) is the symmetric positive definite matrix P , used to calculate the gains K_r in (25). The variables are the plant dynamic G , the symmetric positive semi-definite matrix $Q = C^T C$, and the diagonal symmetric positive definite matrix $R = \rho I_m$ with $\rho \rightarrow 0^+$ and m equal to the system outputs.

$$PA + A^T P + Q - PBR^{-1} B^T P = 0 \quad (24)$$

$$K_r = R^{-1} B^T P \quad (25)$$

3.1.3 Multivariable Stability Margins Theorem

The multivariable stability margins are valid independently and simultaneously for each input of a MIMO system, as stated in the Theorem presented in the works of Prakash (1990), Skogestad and Postlethwaite (1996). Further, since the LQR regulator and the Kalman filter are dual, the Theorem also applies to the Kalman filter theory. Hence, if a TFL compensator is designed using the Kalman filter, the stability margins may be attended for G_{KF} , and the same margins are assured for the transfer function GK due to the recovery proceeding.

Theorem: For an LQR design with matrices $Q > 0$ and $R > 0$, the following multivariable stability margins are guaranteed for a system with m inputs:

- Gain margin: $\theta_i = 0$ and $0.5 \leq k_i \leq \infty$, $i = 1, 2, \dots, m$
- Phase margin: $k_i = 1$ and $|\theta_i| \leq 60^\circ$, $i = 1, 2, \dots, m$

4. KREISSELMEIER'S LOOP

Kreisselmeier's topology in Fig. 9 consists of the nominal plant G_p , subjected to perturbations d and n in low and high frequencies, respectively. A two-degrees of freedom design is possible by suitably choosing the desired dynamics F . Assuming a non-singular transfer function G_p with the same inputs and outputs, Kienitz and Kadiramanathan (2017) demonstrated that selecting $F = G_p^{-1} D$ forces a closed loop response to r equal to D , as stated in (26).

$$y = Dr - (I + G_p R)^{-1} G_p R n + (I + G_p R)^{-1} d \quad (26)$$

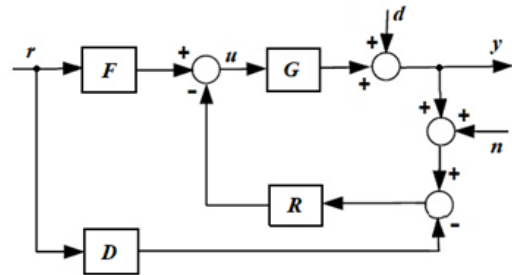


Fig. 9. Kreisselmeier's topology.

5. ROBUST CONTROL DESIGN

The design requirements are defined as in previous works Ramos (2011), Moreira (1995), Kienitz and Moreira (1993):

(r1) Time response to a simultaneous unit step degree in all inputs: null steady state offset, settling time minor than 10 (s), overshoot minor than 10%, and rise time between 0.5 and 1(s);

(r2) Attitude error during flight reference following (except during roll maneuvering) and without wind disturbance: limited to 0.5 (°);

(r3) Actuator's deflection during flight reference following: limited to 1(°) in roll and 3(°) in pitch and yaw;

(r4) Insensitivity to step wind for null inputs: disturbance of 6 (m/s) before 10 (s) and 20 (m/s) between 10 and 50 (s) of flight.

In the next section, the performance barriers are evaluated for each operating point. Subsequently, the TFL/LTR gains are obtained in two operating points: at the instant of 1 second (during lift-off) and at the maximum dynamic pressure (P_{dmax}) around 40 seconds. The compensator calculated at 1 (s) maintains the stability before the transonic regime, which occurs at about 20 and 30 (s), provoking enough change in plant parameters to cause divergence. In that way, if a new operating point were chosen at 20 (s), the complete TFL/LTR procedure had to be repeated. On the other hand, the straightforward approach herein proposed significantly reduces the effort. Finally, in Kreisselmeier's topology, while the function D is equal to the desired time domain transfer function, the controller R is a TFL/LTR compensator responsible for stability and robust performance.

5.1 Performance barrier in low frequencies

The low-frequency performance specification is obtained through the disturbance transfer function G_d (27) considering the linear coupled system $(A, B_d, C, 0)$ in the presence of wind disturbance d .

$$G_d(s) = C(sI - A)^{-1}B_d \quad (27)$$

The performance barrier $1/\alpha_d(\omega)$ is obtained through (13) for each operating point separately, where the breaking point $\omega_d = 5$ (rad/s) is a design choice (Fig. 10). The function $\alpha_d(\omega)$ is obtained assuming that $G_{d\psi} = G_{d\theta}$, once $B_{d\psi} \approx B_{d\theta}$. The wind disturbance has an intensity of 20 (m/s) and the maximum attitude error is limited to 0.5 (°) ≈ 0.00873 (rad).

5.2 Performance barrier in high frequencies

In the specific case of flexible bodies, the performance barrier in high frequencies can be defined with the added objective to work as a filter. So, the barrier's design is based on the flexible modes' gains considering the most critical frequency span, which goes from 26 to 40 (rad/s). In that way, the shape of the barrier $\alpha_n(\omega)$ is selected to be equal to the opposite value of the peak gain (dB) of the first flexible mode, which occurs at 26 (rad/s) and is followed by a constant attenuation of -16,45 (dB). This unique barrier is quite restrictive and attenuates the first and second modes for both operating points.

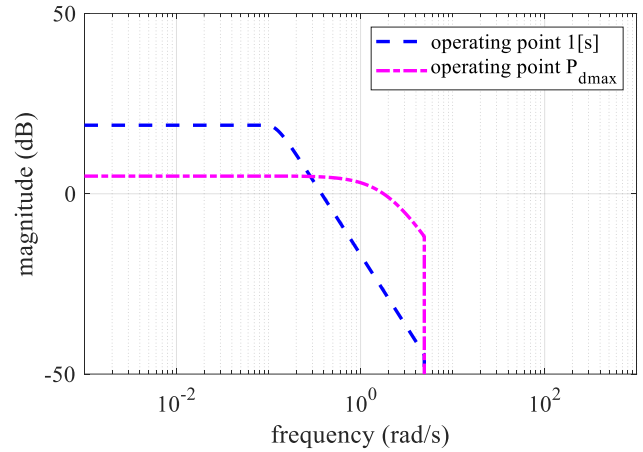


Fig. 10. Performance barriers for each operating point.

5.3 TFL/LTR Compensator Design

5.3.1 Operating point at the instant of 1(s)

At one second of flight, the rigid body coupled linear plant is minimal phase and unstable. The poor behavior of singular values at low frequencies is tackled by augmenting the plant with integrators. In that way, G_{KF} is shaped (Fig. 11) through the adjustment of the main diagonal elements of the positive semi-definite matrix $Q = LL^T$, $L = [L_L \ L_H]^T$. As stated in the stability Theorem, improved margins are guaranteed by the positive definite matrix $Q = \text{diag}(LL^T)$. The objective G_{KF} was obtained for $\mu = 50$.

The singular values of G_{KF} are recovered by GK with a reduction of ρ . Finally, the small gain structure implemented not only offers a smaller control effort u but also a good recovery. The obtained compensator is reduced from an eleventh-order one to a ninth-order (Fig. 12).

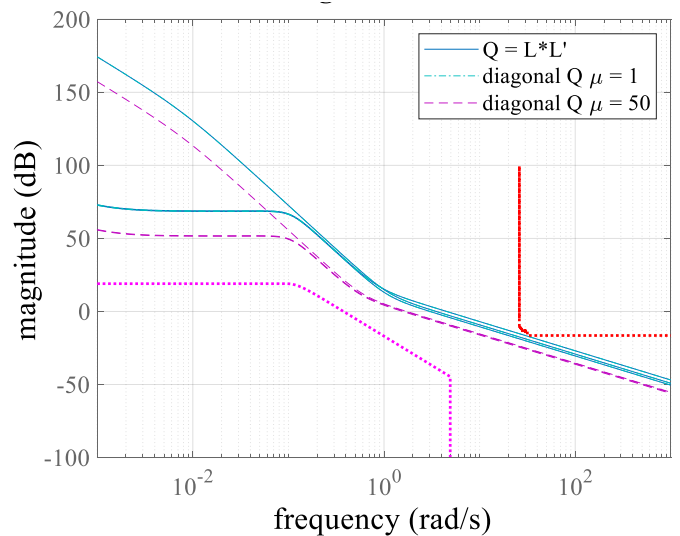


Fig. 11. Frequency response of G_{KF} for the augmented plant at 1(s) operating point while adjusting Q and μ .

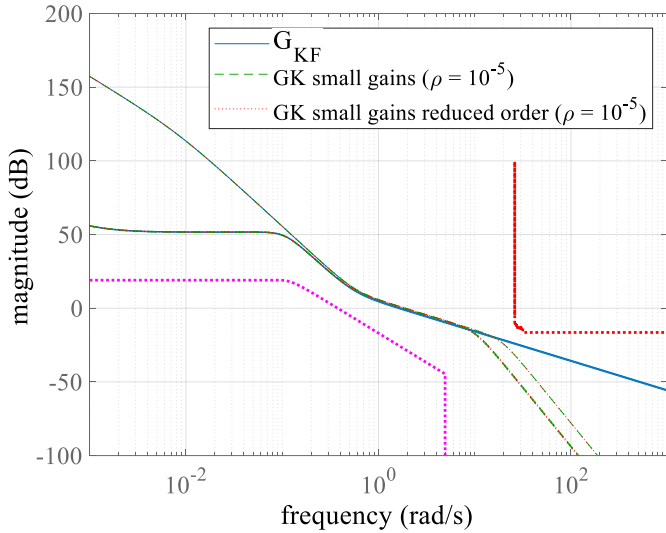


Fig. 12. Singular values recovery using the small gain structure of the compensator at 1 (s) operating point.

5.3.2 Operating point at P_{dmax}

At the instant of maximum dynamic pressure, the system is unstable and has minimal phase. Once again, the augmentation of the plant is needed to correctly shape the curves through the transition region. The target G_{KF} is obtained by changing the main diagonal elements of $Q = LL^T$ and, in sequence, the stability Theorem is used, defining the positive definite matrix Q . The recovery procedure (Fig. 13) employing the small gain structure shows that the shape of GK is suited for $\rho = 10^{-5}$, even with the reduction of the compensator.

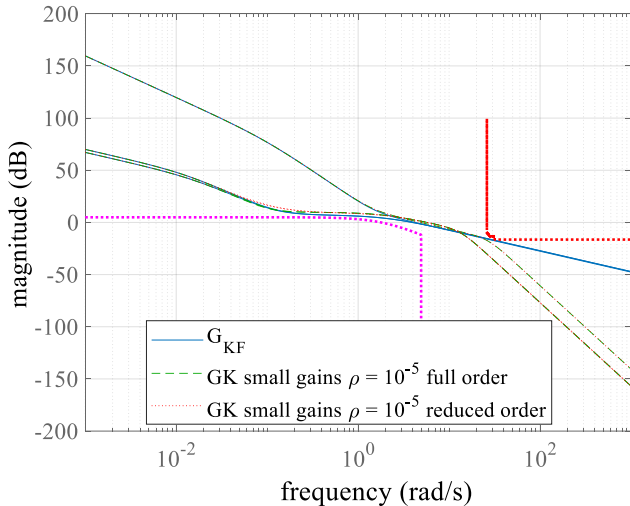


Fig. 13. Singular values recovery using the small gains structure at P_{dmax} .

5.3.3 Interpolation of compensators in 20 (s) of flight

The gains at 20 (s) are updated using interpolation, which avoids the complete TFL/LTR procedure. The singular values of GK show that the performance barriers of the two operating points are respected using the small gain loop (Fig. 14).

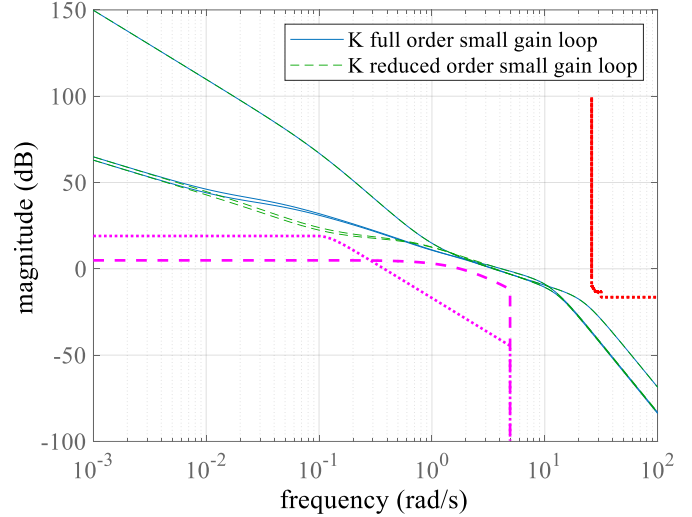


Fig. 14. Singular values of GK obtained in 20 (s) of flight.

5.4 Kreisselmeier's Topology Design

The controller $R(s) = K(s)I_3$ corresponds to the TFL/LTR compensator K in series with the integrators used for the augmentation of the plant. The function D_I is modeled as a second-order transfer function (28) applied simultaneously in the three plant inputs $D(s) = D_1(s)I_3$. At last, the filter $F = G^{-1}D$ is obtained for each operating point.

$$D_1(s) = \frac{\omega_n^2}{s^2 + 2\zeta\omega_n s + \omega_n^2} = \frac{19,67}{s^2 + 7,984s + 19,67} \quad (28)$$

6. RESULTS

Next, the design tests realized in MATLAB are presented and discussed. Firstly, time response is verified in each operating point of the rigid body linear model. In sequence, trajectory following and disturbance rejection are examined for the flexible body nonlinear system.

6.1 Rigid body coupled linear system

The step response requirements (r1) are satisfied, as shown in Fig. 15. Kreisselmeier's topology delivers the same closed-loop response D even when the plant operating point differs.

6.2 Flexible body coupled nonlinear system

The controller gains are updated only three times (at 1, 20, and 40 seconds) during the period of simulation, which reproduces quite similar features of a real rocket flight, once the system herein presented includes variable parameters, flexible modes, and nonlinear actuators. The filter F was maintained fixed at 1(s) operating point. As attack angles and control energy are sufficiently small, the design can deal with even more stressful situations that may be considered.

The control design fulfills the attitude following response needs since requirements for trajectory errors (r2) and deflection (r3) are satisfied, as shown in Fig. 16 to 18.

The system tends to instability around 50 (s), what suggests that the instant of 50 (s) would be a new operating point in

order to continue the stabilization studies and the analysis of the requirements accomplishment.

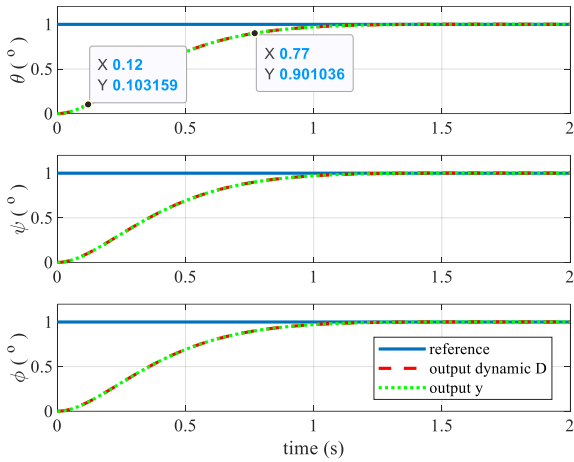


Fig. 15. The unit step response is identical for the two operating points.

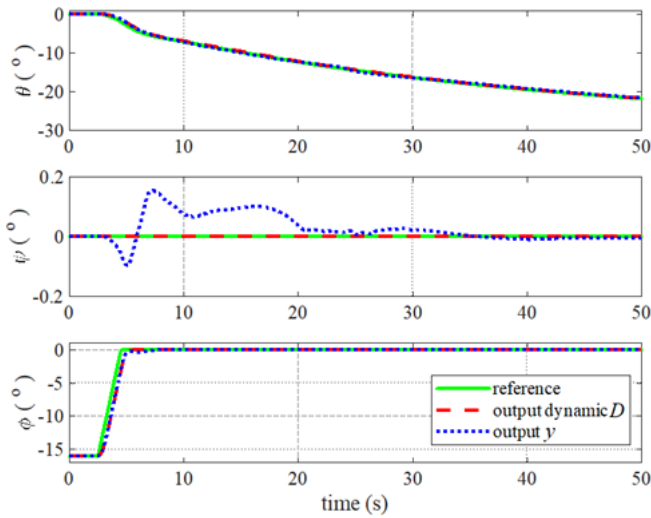


Fig. 16. Trajectory following for pitch (θ), yaw (ψ), roll (ϕ).

6.3 Influence of wind disturbance for the flexible body coupled nonlinear system

The control design demonstrates good robustness to a step disturbance applied in yaw and pitch planes for zeroed inputs (r_4) since control effort and attitude errors are significantly small and tend to zero. Again, the influence of the transonic regime is present at around 25 (s), as seen in Fig. 19.

7. CONCLUSIONS

The robust control design proposed in the present work associates Kreisselmeier's topology with the TFL/LTR procedure to accomplish stability and the design requirements for the VLS launch vehicle. Only three different sets for the TFL/LTR compensator gains are tuned, maintaining the other

parameters of Kreisselmeier's loop fixed during 50 seconds of simulation, using a simplified algorithm that considerably reduced the effort to define suited gains at an instant between the two operating points. One advantage of the controller studied is the attenuation of the vehicle's natural frequencies without adding bending filters. Besides, the robustness in low frequencies is verified for a wind disturbance, that is tackled with a small actuator's deflection. Finally, the control design herein proposed accomplishes extremely well a set of VLS design requirements, presenting excellent results in terms of robust performance and multivariable stability margins, especially considering the asymmetric and changing parameters of the plant. For further work, the results can be tested in any small launch or missile system with similar actuators, like the Microsatellite Launch Vehicle (VLM), for instance.

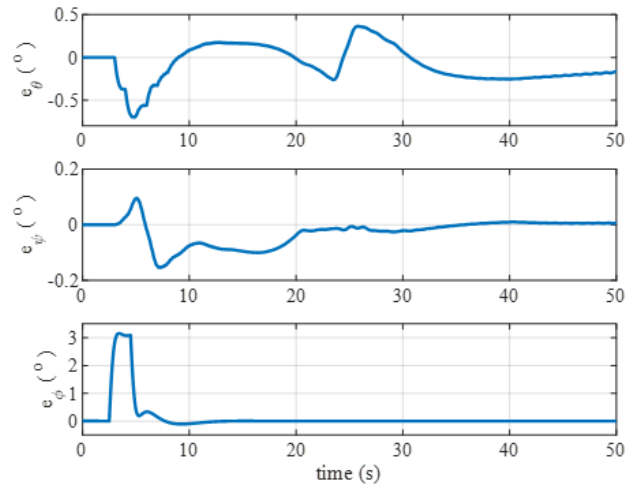


Fig. 17. Attitude error during trajectory following for pitch (e_θ), yaw (e_ψ), and roll (e_ϕ).

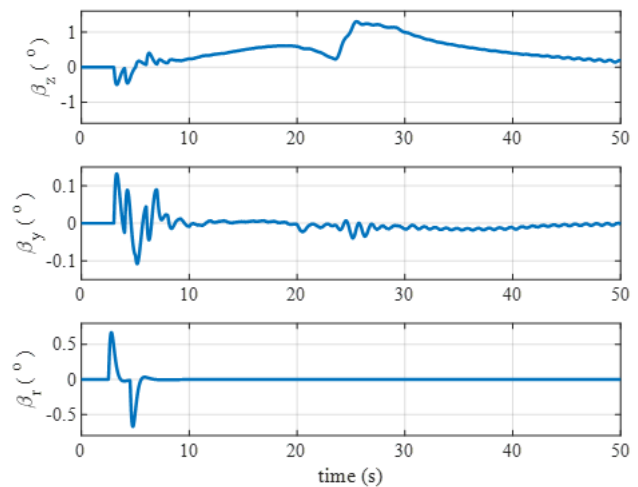


Fig. 18. Control effort demanded by trajectory following for pitch (β_z), yaw (β_y), and roll (β_r).

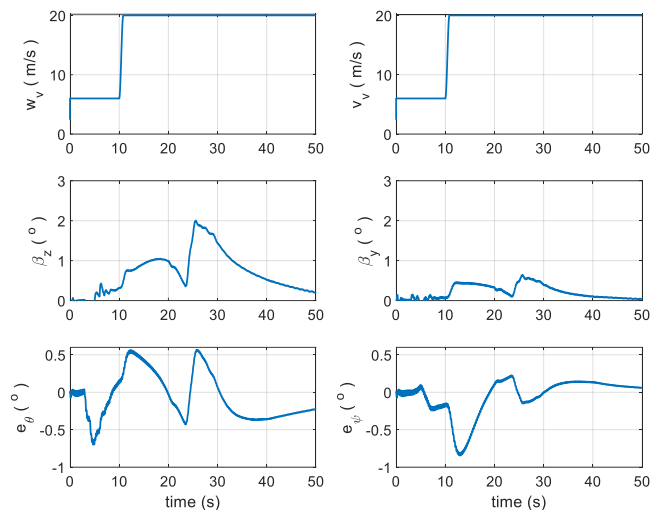


Fig. 19. Attitude error and control effort demanded by a step wind disturbance considering all references null.

ACKNOWLEDGEMENT

The second author acknowledges partial support by CNPq through grant #306900/2018-1.

REFERENCES

- Athans, M. (1986). A tutorial on the LQG/LTR method. In: *American Control Conference (ACC)*, vol. 2, p. 1289-1296, 1986, Seattle, WA, USA. Proceedings [...].
- Cruz, J. J. (1996). *Controle robusto multivariável: O Método LQG/LTR*. São Paulo: Editora da Universidade de São Paulo (Edusp), 163 p.
- Doyle, J. C., Stein, G. (1981). Multivariable feedback design: concepts for a classical/modern synthesis. *IEEE Transactions on Automatic Control*, v. AC-26.
- Dubanchet, V., Saussié, D., Bérard, C., Saydy, L., Gourdeau, R. (2012). Robust control of a launch vehicle in atmospheric ascent based on guardian maps. In: *American Control Conference (ACC)*, p. 938-943, Montréal, Canada.
- Ganet-Schoeller, M., Ducamp, M. (2010). LPV Control for Flexible Launcher. In: *AIAA Guidance, Navigation, and Control Conference*, p. 8193, Toronto, Canada.
- Kienitz, K. H., Kadiramanathan, V. (2017). New insights for applications of Kreisselmeier's structure in robust and fault tolerant control. In: *IEEE Aerospace Conference*, Big Sky, MT, USA. Proceedings [...].
- Kienitz, K. H., Moreira, F. J. O. (1993). *Anteprojeto de algoritmos de controle do VLS com atuadores do tipo tubeira móvel*. Instituto de Aeronáutica e Espaço, São José dos Campos, SP, Brasil. RT-031-ASE-C/93. 1993. In Portuguese.
- Leite Filho, W. C. (2002). Estrutura do Sistema de Controle do VLS. *Revista Controle & Instrumentação*. n 72, p.71-77.
- Lu, B., Falde, D., Iriarte, E., Besnard, E. (2015). Switching robust control for a nanosatellite launch vehicle. *Aerospace Science and Technology*, 42, p. 259-266.

- Mooij, E. (2020). Robust Control of a Conventional Aeroelastic Launch Vehicle. In: *AIAA Scitech 2020 Forum*, p. 1103, Orlando, FL, USA.
- Moreira, F. J. O. (1995). *Projeto de algoritmos de controle do VLS com atuadores do tipo tubeira móvel*. Instituto de Aeronáutica e Espaço, São José dos Campos, SP, Brasil. RT-050-ASE-C/95.
- Navarro-Tapia, D., Marcos, A., Bennani, S., Roux, C. (2016). Structured H-Infinity Control Based on Classical Control Parameters for the VEGA Launch Vehicle. In: *IEEE Conference on Control Applications (CCA)*, p. 33-38, Buenos Aires, Argentina.
- Palmério, A. F. (2017). *Introdução à Tecnologia de Foguetes*. São José dos Campos: SindCT. 304 p. 2017.
- Prakash, R. (1990). *Target Feedback Loop / Loop Transfer Recovery (TFL/LTR) robust control system designs*. 254 p. Doctor of Philosophy (Electrical Engineering) – University of Missouri, Rolla. 1990.
- Ramos, F. O. (2011). *Automation of H_∞ controller design and its observer-based realization*. 154 f. Instituto Nacional de Pesquisas Espaciais (INPE), Institut Supérieur de l'Aéronautique et de l'Espace (ISAE), São José dos Campos (Brasil), Toulouse (França).
- Skogestad, S., Postlethwaite, I. (1996). *Multivariable feedback control*. 2 ed. Chichester: John Wiley & Sons. 572 p.
- Yamada, A. F. C. de S. (2019). *Estratégia de controle para um veículo lançador utilizando múltiplos controladores robustos*. Master's Dissertation. Instituto Tecnológico de Aeronáutica.